Crystal structure of CD155 and electron microscopic studies of its complexes with polioviruses

Ping Zhang[a,1], Steffen Mueller[b,1], Marc C. Morais[a,2], Carol M. Bator[a], Valorie D. Bowman[a], Susan Hafenstein[a], Eckard Wimmer[b], and Michael G. Rossmann[a,3]

[a]Department of Biological Sciences, Purdue University, 915 West State Street, West Lafayette, IN 47907-2054; and [b]Department of Molecular Genetics and Microbiology, Stony Brook University, 280C Life Sciences Building, Stony Brook, NY 11794-5222

Edited by Gregory A. Petsko, Brandeis University, Waltham, MA, and approved October 8, 2008 (received for review August 8, 2008)

When poliovirus (PV) recognizes its receptor, CD155, the virus changes from a 160S to a 135S particle before releasing its genome into the cytoplasm. CD155 is a transmembrane protein with 3 Ig-like extracellular domains, D1–D3, where D1 is recognized by the virus. The crystal structure of D1D2 has been determined to 3.5-Å resolution and fitted into ≈8.5-Å resolution cryoelectron microscopy reconstructions of the virus–receptor complexes for the 3 PV serotypes. These structures show that, compared with human rhinoviruses, the virus–receptor interactions for PVs have a greater dependence on hydrophobic interactions, as might be required for a virus that can inhabit environments of different pH. The pocket factor was shown to remain in the virus during the first recognition stage. The present structures, when combined with earlier mutational investigations, show that in the subsequent entry stage the receptor moves further into the canyon when at a physiological temperature, thereby expelling the pocket factor and separating the viral subunits to form 135S particles. These results provide a detailed analysis of how a nonenveloped virus can enter its host cell.

cell entry | receptor | virus

The ability of a virus to recognize and attach to susceptible cells is essential for the initiation of infection and partially determines viral host specificity, tissue tropism, and pathology. However, successful infection requires not only cell recognition, but also triggers events leading to the release of the genome into the cell. Any study of these first steps in viral infection should, therefore, include structural investigations at the molecular level of interactions between virus and its receptor.

Poliovirus (PV), the causative agent of poliomyelitis, is one of the most thoroughly studied and best-understood viruses to date (1). PVs are members of the *Enterovirus* genus within the *Picornaviridae* family. Picornaviruses also include a number of other significant human pathogens, such as human rhinoviruses (HRVs), coxsackieviruses, echoviruses, enteroviruses, and hepatitis A virus (2). The 3D atomic structures of many picornaviruses have been determined by X-ray crystallography, including those of PV1 (3), PV2 (4), and PV3 (5). Picornaviruses have a diameter of ≈310 Å and have icosahedral symmetry with 60 copies of the viral proteins (VP) VP1, VP2, VP3, and VP4 that encapsidate the 7-kb RNA genome of plus-strand polarity. VP1, VP2, and VP3 (each ≈35 kDa) have similar antiparallel β-barrel "jelly-roll" folds and form the capsid (3, 6). The small VP4 (≈7 kDa) is myristylated at its amino terminus (7, 8) and is located on the inner wall of the capsid.

PV initiates infection when it recognizes and binds to CD155, the only PV receptor known to date (9, 10). Humans are the only natural host of PV, although chimpanzees and Old World monkeys, which express receptors closely related to human CD155, can be experimentally infected (11). Like many other receptor molecules used by picornaviruses, CD155 is a long, highly glycosylated, single-span cell surface molecule belonging to the Ig super family (12). It consists of 3 successive Ig-like domains (D1, D2, and D3), a transmembrane domain and a C-terminal cytoplasmic domain (13) (Fig. 1). The human CD155 gene is expressed in 4 splice variants (α, β, γ, and δ) of which 2 variants (β and γ) are lacking the transmembrane domain and are released from the cell subsequent to their expression. The CD155α and CD155δ isotypes differ only in their cytoplasmic domains and can function as PV receptors (9). Each Ig-like domain of CD155 has a β-barrel fold in which the β-strands (labeled A–G) run parallel or antiparallel to the long axis of the domain.

CD155 is a member of a large class of molecules with Ig-like folds whose predominant function is related to cellular adhesion and activation (14, 15). CD155 also activates natural killer cells (16, 17) and has been reported to play a role in cell motility and tumor cell invasion (18).

The CD155 amino-terminal domain, D1, which is responsible for viral recognition (19, 20), is most closely related to the variable domains in antibodies (21). The fully deglycosylated CD155 can function as a receptor for PV, but is significantly more efficient in mediating PV infection compared with WT CD155 (13). CD155 missing domains D2 and D3 is sufficient for attachment of PV to, and infection of, host cells although with decreased efficiency (22, 23). Therefore, the present studies with the truncated receptor D1D2 are representative of the initial interactions between PV and host cells.

Either membrane-bound CD155 or soluble CD155 (glycosylated or deglycosylated) can convert native PV particles (160S) into altered A-particles (135S) in vitro (24). The A particles have an expanded capsid shell (25) and have the N-terminal extension of VP1 and VP4 externalized. VP4 exits the viral capsid probably via a channel along the 5-fold axes of the capsid, entering the host cell's membrane after cell recognition and thereby initiating infection (26). Longer incubation leads to the formation of 80S particles, which have lost both VP4 and the RNA genome. In vivo, the 135S and 80S particles are intermediates in the PV uncoating pathway (24).

Unlike HRVs, there are only 3 PV serotypes (PV1, PV2, and PV3), possibly the result of highly specific interaction between the receptor and virus, therefore limiting the variability of

Author contributions: P.Z., S.M., M.C.M., E.W., and M.G.R. designed research; P.Z., S.M., C.M.B., and V.D.B. performed research; S.H. contributed new reagents/analytic tools; P.Z. and M.G.R. analyzed data; and P.Z. and M.G.R. wrote the paper.

The authors declare no conflict of interest.

This article is a PNAS Direct Submission.

Data deposition: The atomic coordinates have been deposited in the Protein Data Bank, www.pdb.org (PDB ID codes 3EOW, 3EPC, 3EPF, and 3EPD). The cryoreconstruction maps reported in this paper have been deposited in the Array Express database, www.ebi.ac.uk/arrayexpress (accession nos. 6390, 6386, and 6387).

[1]P.Z. and S.M contributed equally to this work.

[2]Present address: Sealy Center for Structural Biology and Molecular Biophysics, University of Texas Medical Branch, 301 University Boulevard, Galveston, TX 77555-0647.

[3]To whom correspondence should be addressed. E-mail: mr@purdue.edu.

This article contains supporting information online at www.pnas.org/cgi/content/full/0807848105/DCSupplemental.

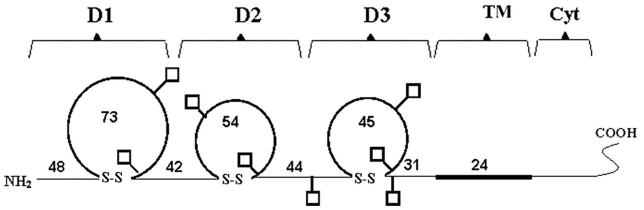

Fig. 1. Schematic presentation of human CD155α. The ectodomain is divided into the Ig-like D1, D2, and D3 domains (circles), followed by the transmembrane (TM) domain and the cytoplasmic domain (Cyt). The number of amino acids within each structural segment is indicated. The predicted N-glycosylation sites are depicted as open squares.

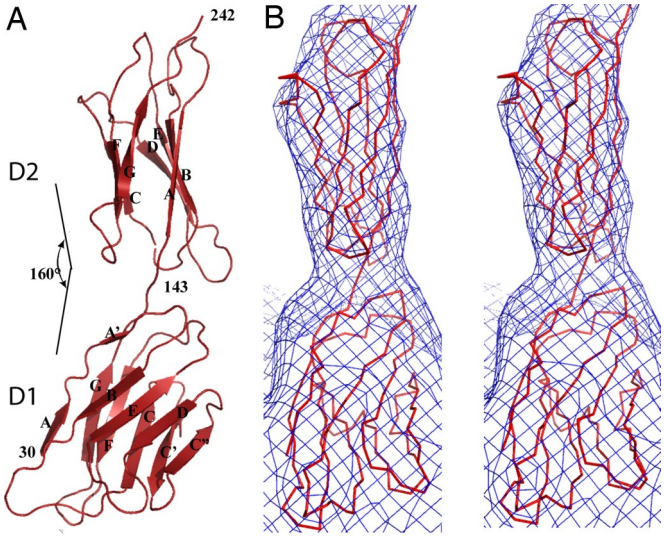

Fig. 2. The structure of domains 1 and 2 of CD155. (*A*) The β-strands in D1 and D2 are labeled A–F using the normal nomenclature for a ''variable'' and ''constant'' Ig-like fold, respectively (21). The 160° elbow angle between domains D1 and D2 is shown. (*B*) The Cα backbones (red) of the fitted D1 and D2 domains are shown in the CD155-PV1 cryoEM density (blue). The elbow angle between D1 and D2 found in crystal structure has been adjusted to fit in the cryoEM density.

residues in the receptor binding surface. A narrow surface depression around the 5-fold axes, the ''canyon,'' circumscribes the pentameric vertices (6). It was suggested that the site of receptor attachment would involve the more conserved amino acid residues in the canyon, a site that is protected from host immune surveillance by the inability of neutralizing antibodies to penetrate far into the canyon. Although the ''canyon hypothesis'' was challenged (27) because of the later discovery that antibody footprints and the receptor binding site could partially overlap, the prediction has been substantiated by cryoelectron microscopic (cryoEM) studies of many picornavirus–receptor interactions (28).

A fatty acid-like molecule known as the ''pocket factor'' was observed to bind into a hydrophobic pocket beneath the canyon in HRVs and PVs (28). Binding of the receptor into the canyon probably competes with the binding of the pocket factor into the hydrophobic pocket. Release of the pocket factor destabilizes the virus and thereby initiates uncoating (29). Replacement of the pocket factor by antiviral compounds can inhibit both attachment and uncoating (29, 30).

The cryoEM studies (31–34) of PVs complexed with their receptor CD155 were, at best, 16-Å resolution and were limited by the need to use homology models for CD155 that were based on Ig-like molecules that had <25% amino acid identity. The inaccuracy of the homology models would have influenced the determination of the contact residues in the virus–receptor interface. Here, we report the crystal structure of deglycosylated CD155 D1D2, which was fitted into the 8- to 9-Å resolution cryoEM reconstructions of each PV serotype complexed with CD155. The crystal structure of the truncated CD155 receptor was useful for investigating the interaction of CD155 with PV, but will also be useful for analyzing the interactions between CD155 and its cellular binding partners.

Results and Discussion

The Structure of CD155. Earlier cryoEM reconstructions of PV-CD155 complexes (32, 33) had shown that D3 is generally of lower density, suggesting that the hinge between D2 and D3 is flexible. Because the hinge region might have been an obstacle for growing crystals of CD155 ectodomain, a gene construct was made that contained a 27-aa signal peptide followed by D1 and D2 with a C-terminal $(His)_6$ tag. Furthermore, the 5 putative glycosylation sites were altered to stop glycosylation (see *Materials and Methods*). Plaque reduction assays [supporting information (SI) Text] showed the His-tagged, deglycosylated D1D2 sample reduced the number of plaques 95%, 98%, and 97% when assaying PV1, PV2, and PV3, respectively. This result should be compared with the 100% plaque reduction when using fully glycosylated D1D2D3 against PV1.

The D1D2 structure (Tables S1 and S2) (Fig. 2*A* and Fig. S1) has a total length of ≈80 Å. Domain 1 (residues 30–143) has a diameter of ≈20 Å and domain 2 (residue 144–242) has a diameter of ≈15 Å, with an interdomain ''elbow'' angle of ≈160° between the long axes of the 2 domains. Domain 1 belongs to the variable (V) set of Ig super family (IgSF) domains (21) that has 2 extra β-strands, C′ and C″, between β-strands C and D forming a β-sandwich with 1 sheet consisting of the AA′BED strands and the other of the GFCC′C″ strands. Domain 2 belongs to the constant (C2) set of IgSF domains with an ABED and a CFG sheet.

Three earlier structural studies (31, 32, 34) had examined the interaction of PV with its receptor by using homology models in place of the actual PV receptor. Comparison of these homology models (31, 32) with the structure of CD155 reported here gave rmsd between equivalent Cα atoms in D1 of 3.6 and 3.1 Å, respectively, with the largest differences (up to 13.6 Å between Cα atoms) being in the CC′, C″D, DE, and FG loops. All of these loops are in the virus–receptor interface. Although D2 is a ''constant'' type Ig domain, the superimposable Cα atoms in D2 have even larger rmsd of 4.6 and 4.1 Å, respectively. The biggest differences in the D2 domains are in the predictions of the loops connecting β-strands. Comparison of the CD4 model used by Xing *et al.* (34) with the actual structure of CD155 reported here showed only 60% and 51% of the protein sequences could be structurally equivalenced in D1 and D2, respectively. These observations show that the homology models used for the previous interpretations of the cryoEM PV–CD155 complex densities had large errors in which amino acids were wrongly positioned by as much as ≈3 times the distance between adjacent amino acids. Thus, although homology models can be useful, they can also be inaccurate.

Fitting the CD155 Structure into cryoEM Densities. The structure of CD155 was fitted into the cryoEM densities of the PV1, PV2, and PV3 receptor complexes (see *Materials and Methods*) (Fig. 3 and Fig. S2) using the computer program EMfit (35) (Fig. 2*B* and Fig. S3). The *sumf* values (a measure of the quality of the fit; see *Materials and Methods*) when domain D1 was fitted into the PV1, PV2, PV3–CD155 complex cryoEM densities are ≈0.73, 0.85, and 0.84 of the *sumf* values found when fitting the VP1–VP2–VP3–VP4 protomer into the cryoEM density of each virus (Tables S3–S6). The ratios of the *sumf* values of domain D2

BIOCHEMISTRY

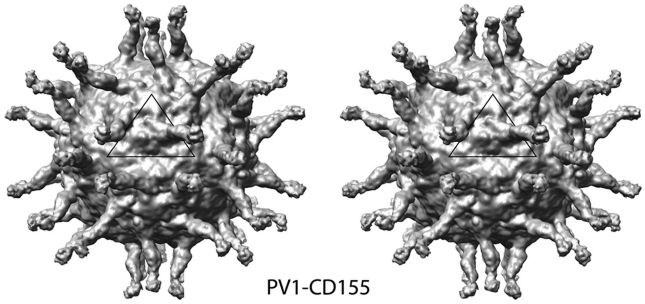

Fig. 3. Stereoviews showing the cryoEM reconstructions of PV1 complexed with deglycosylated CD155, viewed down an icosahedral 2-fold axis (Tables S1 and S2). The black triangle defines 1 icosahedral asymmetric unit on the viral surface.

compared with the protein shell are ≈0.4, 0.6, and 0.6 in the 3 complexes, respectively. Both of these results suggest that the PV2 and PV3 complexes have higher receptor occupancy than the PV1–CD155 complex (Table S6). The declining density along the length of the CD155 molecule may be caused by the flexibility of the CD155 molecule or slight misalignments of the images that went into the cryoEM reconstructions.

A comparison of the 3 EM-fitted CD155 D1D2 structures reported here showed that they are closely similar to each other with rmsd of 0.4–0.7 Å between equivalent Cα atoms (Table S7) with the largest differences being only 2.5 Å. However, comparison of these EM-fitted structures with the crystal structure of CD155 D1D2 gave a rmsd between equivalent Cα atoms of 2.4–2.6 Å, with the largest differences being as much as 7.6 Å (Table S7). Moreover, when the cryoEM-fitted structures of CD155 were compared with each other by superimposing domain D1, the rotation angle between any 2 D2 domains varied by <10.9°. However, in comparing the cryoEM structures with the crystal structure, the angles between the D2 domains were >15.9° (Fig. S2*C*) (Table S8). Apparently, the cryoEM-fitted CD155 molecules represent the natural low-energy state of CD155, whereas the crystal structure has been slightly distorted, presumably by the crystal lattice forces. The presumably lower energy and more stable form of the cryoEM-fitted structures compared with the crystal structure may be the result of Ser-227 in the FG loop and the hinge residue Lys-144 of domain D2 being closer to Phe-40 in βA of domain D1 than they are in the crystal structure. As a result, the shortest interdomain distance is 3.1 Å in the cryoEM structures compared with 5.3 Å in the crystal structure (Fig. S2*C*).

A comparison of the position and orientation of CD155 with respect to the icosahedral axes that define the virus coordinates in each of the 3 viruses (Fig. S2*D* and (Tables S9–S11) showed that they have a rmsd of 0.7–1.5 Å between equivalent Cα atoms in D1 (Table S10). Thus, the positions and orientations of domain D1 on the viral surfaces are apparently the same within experimental error. However, the rmsd between equivalent Cα atoms among the D2 domains showed that there is small systematic translation perpendicular to the length of the domain of ≈2.4–2.7 Å between D2 in PV1 compared with D2 in PV2 or PV3 (Fig. S2*D* and Table S11). This observation is supported by the decrease in *sumf* when the docked position of D2 taken from 1 virus was applied to another (Table S12).

Footprint of CD155 Onto the Surface of PVs. Domain D1 leans "eastward" in the canyon and is more tangential than radial with respect to the viral surface. However, domain D2 is oriented more radially than tangentially because of the ≈155° elbow angle between the domains. The interface between CD155 and virus consists of the end loops (CC′, DE, FG), side strands (C, C′, C″), and side loop EF of D1 lying in the canyon. The footprint of CD155 on the viral surface of PVs was mapped in terms of those residues in the virus that had atoms closer than 4 Å from any atom in the bound receptor (Fig. S4). The footprint of CD155 onto the virus was well within the canyon, as had been observed (31–34), and consisted of 3 roughly separate regions: in the "north," "southwest," and "southeast" of the canyon. Although the north and southwest regions are linked with each other in the base of the canyon, the southeastern region is separated by ≈10 Å (Fig. S4) from the other 2 regions. The calculated area of contact between CD155 and the PV surface is ≈1,320 Å^2 (Table S13). In comparison, the area of contact between intercellular adhesion molecule-1 (ICAM-1) and HRVs is only ≈900 Å^2 (36, 37). The larger surface area used by CD155 in making contacts with PV would require that more surface residues need to be conserved to retain the receptor-binding activity. Thus, the more stringent selection of viable mutants that maintain their ability to bind to CD155 would also limit the variability of change in the surface residues that interact with neutralizing antibodies. Hence, the larger interface of CD155 with PVs might explain why there is a more limited set of PV serotypes compared with HRVs.

The interactions described above are consistent with mutational analyses of CD155 (19, 20, 38–43) (Fig. 4 and Table S14) in that all of the mutations that affect receptor binding are on or very close to the residues identified as being in the virus–receptor interface. Similarly, residues that have been mutated, but are not in the interface, do not impact the ability of the receptor to bind

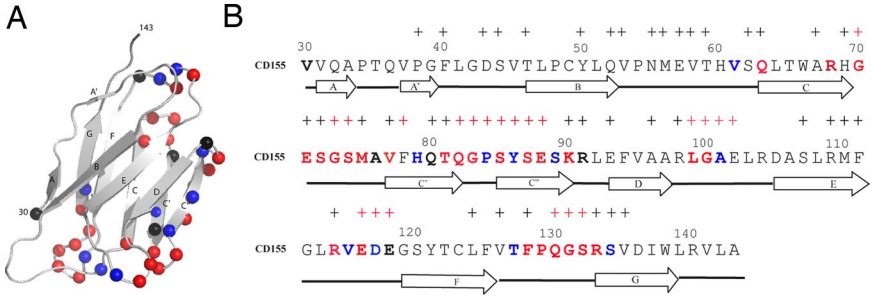

Fig. 4. Mutational studies of CD155 domain D1. (*A*) Ribbon diagram of D1. Residues in the virus–receptor binding interfaces are shown as colored spheres. Residues identified as being in the interface in only 1 serotype are shown in black, residues identified in 2 serotypes are in blue, and residues identified in all 3 serotypes are in red. (*B*) Amino acid sequence and the secondary structural elements of CD155 in D1. Residues are colored as in *A*. Residues that have no impact on CD155 binding, as shown by mutagenesis studies, are labeled with a black +. Residues that have impact on CD155 binding, as shown by mutagenesis studies, are labeled with a red +. The strong correlation between colored amino acids with a red + (residues that impact CD155 binding) is visually evident. Similarly, there is an obvious correlation between residues that have been mutated, but are not in the virus–CD155 interface with a black + (residues that do not impact CD155 binding).

to the virus. Furthermore, changes of CD155 residues in the contact area mostly have reduced binding affinity to PV (Table S14).

The interaction between HRVs and coxsackie A21 with ICAM-1 is determined primarily by complementary charge interactions (36). In contrast, most interactions between the receptor and PV are hydrophobic (Table S13). There is only 1 complementary ion pair (Glu-88 in CD155 with Lys-1297 in PV1, Lys-1296 in PV2, Lys-1297 in PV3) that is conserved in PV1, PV2, and PV3 with an additional ion pair in PV3 (Arg-91 in CD155 with Glu-1296). These ion pairs are between the residues situated along the side of CD155 D1 and residues in the southeast region of the canyon, representing a contact area that does not exist in HRVs. The dominance of hydrophobic interactions between PV and receptor suggests that PV is more able to withstand a change in pH environment without altering its ability to recognize its cellular receptor.

Incubation of PV with HeLa cells at 4 °C leads to the formation of CD155/virus complexes whose formation is reversible with salt solutions, suggesting that the southeast part of the canyon, where there is the only electrostatic interaction between virus and receptor, participates in the initial binding step (33). At 37 °C, however, the formation of virus/receptor complexes is no longer reversible, indicating that at higher temperatures the binding proceeds to a second step in which the pocket factor, below the northern hydrophobic region of the receptor footprint, is expelled.

Pocket Factor. The presence of antiviral compounds in the VP1 pocket stabilize the virus and thereby inhibit both attachment and uncoating (29, 30). It has been hypothesized that the binding of CD155 to PVs displaces the pocket factor and thereby destablizes the virus to initiate uncoating. Indeed, residues that change their conformation in the presence of pocket factor (Table S15 and *SI Text*) overlap with the northern region of the CD155 footprint (Fig. S4). Reduced stability of the virus as the result of binding CD155 has also been demonstrated by incubating CD155 with PVs for many hours or at elevated temperatures, which causes the viruses to disassociate. Thus, the results presented here probably relate to early events of CD155 binding before the expulsion of the pocket factor. Furthermore, it has been shown that binding of CD155 to PVs is a 2-step process (44, 45). Thus, presumably, the present EM studies represent the first of these steps where the release of free energy when CD155 binds to the virus is insufficient to overcome the energy barrier between the initial recognition event and the formation of the subsequent intermediates in the infection process. However, in vivo virus infection would occur at physiological temperature where the initial binding releases enough energy to smoothly continue along the infection pathway. Hence, it was necessary to verify whether the pocket factor is retained in the virus during the first recognition step of virus infection.

Difference maps (Fig. 5) were calculated between the EM reconstruction of the PV1-CD155 complex at 9-Å resolution and an electron density map based on the known atomic structure of PV1 empty capsid (without the presence of the pocket factor) complexed with the known structure of CD155 (*SI Text*). The difference map clearly showed the presence of an elongated pocket factor (Fig. 5*C*). Thus, the current cryoEM results represent an early binding event where the receptor has not penetrated to the base of the canyon and has not yet displaced the pocket factor. Belnap *et al.* (31) suggested that the pocket factor is probably missing in their 21-Å resolution cryoEM map of the PV1–CD155 complex, which is surprising because it was difficult to recognize the pocket factor density at the resolution of their studies (*SI Text*).

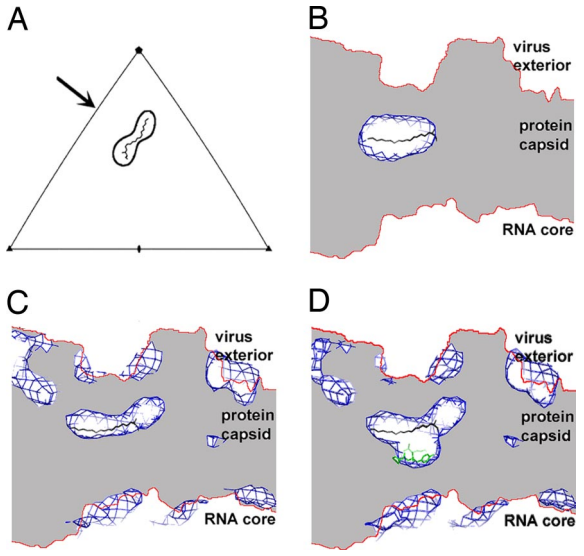

Fig. 5. Pocket factor density. (*A*) Diagrammatic view of the pocket factor position within the reference icosahedral asymmetric unit. The arrow shows the direction of viewing the difference maps in *B–D*. (*B*) The control showing a 10-Å-thick slab of the difference map at 9-Å resolution between the electron density generated from the known PV-CD155 atomic structure with and without the presence of the pocket factor (see *Materials and Methods*). The pocket factor density (contoured at a 15σ level) in the difference map is much bigger than the largest noise peak (which has a height of 1.7σ level) and showed the characteristic elongated shape of the pocket factor. The labels ''virus exterior'' and ''RNA core'' define the radial edge of the capsid shell. The edges of the capsid structure are indicated by continuous red lines. (*C*) The actual difference map at 9-Å resolution between the EM-reconstruction of the PV–CD155 complex and the electron density map based on the known PV–CD155 atomic structure without the presence of the pocket factor. The difference map showed the presence of the pocket factor in the PV–CD155 complex, and significant density at the internal and external edges of the capsid protein. (*D*) A further control map at 9-Å resolution in which the calculated structure omitted 5 aa (residues 1197–1201). This difference map showed positive density at the site of the pocket factor and at the site of the missing residues (colored green), and essentially the same positive and negative noise density in the regions outside the PV protein capsid.

Mutagenesis Analyses of PV. In general, mutations (other than conservative changes) that are in the receptor footprint affect CD155 binding (magenta residues in Fig. 6*A*) and viral replication (19, 20, 38–43) (Table S14). Conversely, mutations that are not in the footprint do not have any effect (yellow residues in Fig. 6*A*). However, some mutations that are not in the footprint do alter the interaction between virus and the receptor (black residues in Fig. 6*A*). All of these residues are in the vicinity of the pocket factor or in the interface between the VP1, VP2, and VP3 subunits, suggesting that the residues in the interface become exposed to the receptor as a consequence of virus–receptor interaction.

The position of CD155 in the canyon was docked to the 135S structure of PV1 by assuming it to be in the same position as in the CD155-PV1 complex relative to the icosahedral axes (Protein Data Bank ID code 1XYR) to investigate what would be the second step of receptor binding once the pocket factor has been expelled and the floor of the canyon has been depressed. The footprint of CD155 onto the 135S (as opposed to 160S) particle surface shows that most of the residues that were identified by mutagenesis studies to affect CD155 binding are in contact with the receptor (Table S16). Thus, the mutagenesis studies are consistent with the formation of the 135S particle (25) and suggest that CD155 moves further into the canyon, causing separation of the subunits from each other in the second binding step (Fig. 6*B*).

BIOCHEMISTRY

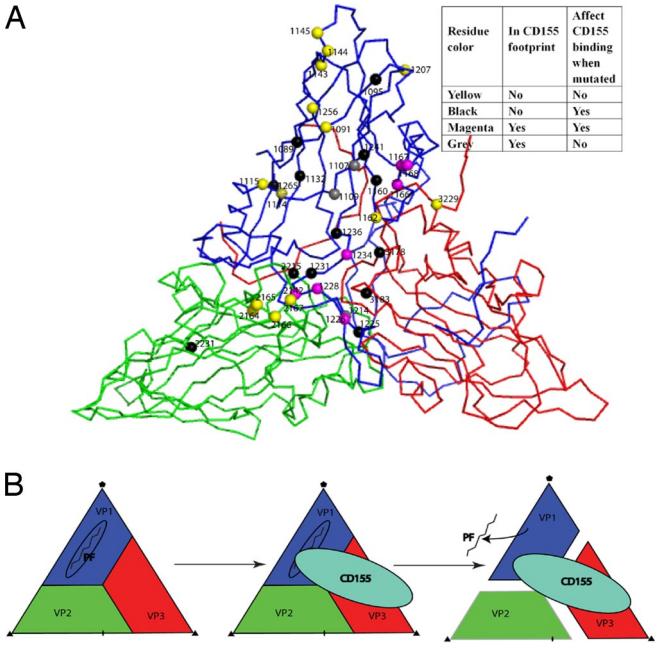

Fig. 6. Mutational studies of PV1. (*A*) The Cα backbone of VP1, VP2, and VP3 in 1 icosahedral asymmetric unit are colored blue, green, and red respectively. Residues that have been mutated and characterized are colored yellow, black, magenta, or gray. Residues that are not in the footprint and do not affect CD155 binding when mutated are colored yellow. The impact on CD155 binding when mutating PV1 residues is color-coded as shown. In general, residues that are not in the CD155 footprint do not affect CD155 binding (yellow spheres). Also, residues that are in the CD155 footprint do affect CD155 binding (magenta spheres). However, there are some residues that are not in the CD155 footprint but do affect CD155 binding (black spheres). These black-labeled residues all are in the vicinity of the pocket factor or in the interfaces between the viral subunits, suggesting that these become available to CD155 subsequent to the first binding event. (*B*) A diagrammatic representation of CD155 interacting with PV. Ovals, triangles, and pentagons indicate the positions of the 2-, 3-, and 5-fold axes, respectively. During the first recognition stage of PV by CD155, the pocket factor (PF) stays in the hydrophobic pocket in VP1. The interaction between PV and CD155 results in the expulsion of the pocket factor, thereby decreasing the stability of the virus and permitting CD155 to move further into the canyon and causing a separation of the viral subunits. This causes exposure of residues that were previously hidden in the interface between the VPs, consistent with the earlier structural studies of 135S particles (25).

There is only 1 mutational study of CD155 that significantly differentiates the 3 PV serotypes (40) (Table S14). The Q130G/GD mutant in the FG loop abolishes receptor binding to PV1 and PV2, but not PV3, although binding to PV3 does not lead to viral infection. The present results show that Gln-130 interacts with the main-chain atoms of residue 1107 on the virus surface that forms part of the hydrophobic interior of the drug binding pocket. Residue 1107 alters its conformation when the pocket factor is expelled. Thus, the mutant, in which Gln is changed to Gly, would probably still be able to bind to the virus but would not have the capacity to interact with residue 1107 and, therefore, not be able to expel the pocket factor, rendering the virus unable to alter its stability as required for uncoating. However, on mutating the neighboring residue Gly-131 to Asp in CD155, Glu-1168 in PV1 would be repelled, thus abolishing CD155 binding to PV1, and Lys-1168 in PV3 would form an ion pair with Asp in the mutated CD155. Thus, CD155 would still be able to bind to PV3, consistent with observation.

Comparison of PVs, HRVs, and Coxsackievirus A21 (CVA21) Receptor-Binding Modes. Among known picornavirus structures, PVs, HRVs, and CVA21 have the greatest sequence and structural similarities. CVA21 and PVs both belong to the *Enterovirus* genus, whereas rhinoviruses have been classified into another genus. Nevertheless, CVA21 and the major group of HRVs recognize ICAM-1 as their cellular receptor (36, 37), whereas PVs use CD155.

The 114-residue D1 domain of CD155 has an Ig-like V fold and differs from the 84-residue domain of ICAM-1, which has an Ig-like intermediate (I) fold lacking the C′ and C″ strands. If the β-strands of CD155 D1 are superimposed on the equivalent strands of ICAM-1 D1 when docked to HRV or CVA21, then the additional C′ and C″ strands in CD155 would have steric conflict with the south side or the north side of the canyon, respectively. Thus, CD155 would be unable to bind to HRVs and CVA21 in a manner similar to how ICAM-1 binds to these viruses. Similarly, binding of ICAM-1 to the site of CD155 in PVs would have steric problems, accounting for the inability of ICAM-1 to bind to PVs.

Viral Entry. The results reported here show that during the initial binding of CD155 to PV residues in the FG loop of CD155 D1 exert a force on the roof of the pocket in VP1, resulting in the expulsion of the pocket factor. Loss of the hydrophobic pocket factor permits CD155 to move further into the canyon to increase its binding affinity and decreases the stability of the virus (44), causing a separation of the viral subunits. This process initiates uncoating (26) via the 135S (25) particle intermediate and triggers the release of the genomic RNA (46).

Materials and Methods

Detailed experimental procedures are provided in *SI Text*. In brief, mutated CD155 D1D2 was cloned and expressed in human embryonic kidney cells. The deglycosylated protein was purified by means of affinity chromatography. The structure was solved by using SIRAS phase determination method to 4.0-Å resolution based on Pt derivative. The native structure could then be refined to 3.5-Å resolution. CryoEM reconstructions of PV1, PV2, and PV3 complexed with deglycosylated CD155 were computed to ≈8.5-Å resolution. The D1D2 crystal structure was fitted to cryoEM difference maps in which the PV structures had been subtracted.

ACKNOWLEDGMENTS. We thank Sheemei Lok for helpful suggestions on how to prepare the antibody for purifying CD155; Kyung Choi and Ye Xiang for crystallographic advice; Chuan Xiao for cryoEM reconstruction advice; Sheryl Kelly and Cheryl Towell for help in preparation of the manuscript; Paul Chipman and Yongning He for their earlier cryoEM data collection (32, 33); and the staff of beam line 23D at the Advance Photon Source synchrotron (Argonne,IL). This work was supported by National Institutes of Health Grants AI 11219 (to M.G.R.) and AI 039485 (to E.W.).

1. Semler BL Wimmer E, eds (2002) *Molecular Biology of Picornaviruses* (Am Soc Microbiol, Washington, DC).
2. Melnick JL (1996) Enteroviruses: Polioviruses, coxsackieviruses, echoviruses, and newer enteroviruses. *Fields Virology*, eds Fields BN, Knipe DM, Howley PM (Lippincott–Raven, Philadelphia), 3rd Ed, pp 655–712.
3. Hogle JM, Chow M, Filman DJ (1985) Three-dimensional structure of poliovirus at 2.9-Å resolution. *Science* 229:1358–1365.
4. Lentz KN, *et al.* (1997) Structure of poliovirus type 2 Lansing complexed with antiviral agent SCH48973: Comparison of the structural and biological properties of the three poliovirus serotypes. *Structure* 5:961–978.
5. Hiremath CN, Grant RA, Filman DJ, Hogle JM (1995) The binding of the antiviral drug WIN51711 to the Sabin strain of type 3 poliovirus: Structural comparison with drug binding in rhinovirus 14. *Acta Crysallogr D* 51:473–489.
6. Rossmann MG, *et al.* (1985) Structure of a human common cold virus and functional relationship to other picornaviruses. *Nature* 317:145–153.
7. Chow M, *et al.* (1987) Myristylation of picornavirus capsid protein VP4 and its structural significance. *Nature* 327:482–486.
8. Paul AV, Schultz A, Pincus SE, Oroszlan S, Wimmer E (1987) Capsid protein VP4 of poliovirus is N-myristoylated. *Proc Natl Acad Sci USA* 84:7827–7831.
9. Koike S, *et al.* (1990) The poliovirus receptor protein is produced both as membrane-bound and secreted forms. *EMBO J* 9:3217–3224.
10. Mendelsohn CL, Wimmer E, Racaniello VR (1989) Cellular receptors for poliovirus: Molecular cloning, nucleotide sequence, and expression of a new member of the immunoglobulin superfamily. *Cell* 56:855–865.
11. Mueller S, Wimmer E, Cello J (2005) Poliovirus and poliomyelitis: A tale of guts, brains, and an accidental event. *Virus Res* 111:175–193.

12. Rieder E, Wimmer E (2002) Cellular receptors of picornaviruses: An overview. *Molecular Biology of Picornaviruses*, eds Semler BL Wimmer E (Am Soc Microbiol, Washington, DC), pp 61–70.
13. Bernhardt G, Bibb JA, Bradley J, Wimmer E (1994) Molecular characterization of the cellular receptor for poliovirus. *Virology* 199:105–113.
14. Mueller S, Wimmer E (2003) Recruitment of nectin-3 to cell–cell junctions through transheterophilic interaction with CD155, a vitronectin and poliovirus receptor that localizes to $\alpha_v\beta_3$ integrin-containing membrane microdomains. *J Biol Chem* 278:31251–31260.
15. Ogita H, Takai Y (2006) Nectins and nectin-like molecules: Roles in cell adhesion, polarization, movement, and proliferation. *IUBMB Life* 58:334–343.
16. Bottino C, *et al.* (2003) Identification of PVR (CD155) and nectin-2 (CD112) as cell surface ligands for the human DNAM-1 (CD226)-activating molecule. *J Exp Med* 198:557–567.
17. Fuchs A, Cella M, Giurisato E, Shaw AS, Colonna M (2004) Cutting edge: CD96 (tactile) promotes NK cell-target cell adhesion by interacting with the poliovirus receptor (CD155). *J Immunol* 172:3994–3998.
18. Sloan K, *et al.* (2004) CD155/PVR plays a key role in cell motility during tumor cell invasion and migration. *BMC Cancer* 4:73.
19. Bernhardt G, Harber J, Zibert A, deCrombrugghe M, Wimmer E (1994) The poliovirus receptor: Identification of domains and amino acid residues critical for virus binding. *Virology* 203:344–356.
20. Morrison ME, He Y-J, Wien MW, Hogle JM, Racaniello VR (1994) Homolog-scanning mutagenesis reveals poliovirus receptor residues important for virus binding and replication. *J Virol* 68:2578–2588.
21. Chothia C, Jones EY (1997) The molecular structure of cell adhesion molecules. *Annu Rev Biochem* 66:823–862.
22. Selinka HC, Zibert A, Wimmer E (1991) Poliovirus can enter and infect mammalian cells by way of an intercellular adhesion molecule 1 pathway. *Proc Natl Acad Sci USA* 88:3598–3602.
23. Selinka HC, Zibert A, Wimmer E (1992) A chimeric poliovirus/CD4 receptor confers susceptibility to poliovirus on mouse cells. *J Virol* 66:2523–2526.
24. Hogle JM (2002) Poliovirus cell entry: Common structural themes in viral cell entry pathways. *Annu Rev Microbiol* 6:677–702.
25. Bubeck D, *et al.* (2005) The structure of the poliovirus 135S cell entry intermediate at 10-Å resolution reveals the location of an externalized polypeptide that binds to membranes. *J Virol* 79:7745–7755.
26. Bubeck D, Filman DJ, Hogle JM (2005) Cryoelectron microscopy reconstruction of a poliovirus–receptor–membrane complex. *Nat Struct Mol Biol* 12:615–618.
27. Smith TJ, Chase ES, Schmidt TJ, Olson NH, Baker TS (1996) Neutralizing antibody to human rhinovirus 14 penetrates the receptor-binding canyon. *Nature* 383:350–354.
28. Rossmann MG, He Y, Kuhn RJ (2002) Picornavirus–receptor interactions. *Trends Microbiol* 10:324–331.
29. Rossmann MG (1994) Viral cell recognition and entry. *Protein Sci* 3:1712–1725.
30. Smith TJ, *et al.* (1986) The site of attachment in human rhinovirus 14 for antiviral agents that inhibit uncoating. *Science* 233:1286–1293.
31. Belnap DM, *et al.* (2000) Three-dimensional structure of poliovirus receptor bound to poliovirus. *Proc Natl Acad Sci USA* 97:73–78.
32. He Y, *et al.* (2000) Interaction of the poliovirus receptor with poliovirus. *Proc Natl Acad Sci USA* 97:79–84.
33. He Y, *et al.* (2003) Complexes of poliovirus serotypes with their common cellular receptor, CD155. *J Virol* 77:4827–4835.
34. Xing L, *et al.* (2000) Distinct cellular receptor interactions in poliovirus and rhinoviruses. *EMBO J* 19:1207–1216.
35. Rossmann MG, Bernal R, Pletnev SV (2001) Combining electron microscopic with X-ray crystallographic structures. *J Struct Biol* 136:190–200.
36. Kolatkar PR, *et al.* (1999) Structural studies of two rhinovirus serotypes complexed with fragments of their cellular receptor. *EMBO J* 18:6249–6259.
37. Xiao C, *et al.* (2005) The crystal structure of coxsackievirus A21 and its interaction with ICAM-1. *Structure* 13:1019–1033.
38. Aoki J, Koike S, Ise I, Sato-Yoshida Y, Nomoto A (1994) Amino acid residues on human poliovirus receptor involved in interaction with poliovirus. *J Biol Chem* 269:8431–8438.
39. Colston E, Racaniello VR (1994) Soluble receptor-resistant poliovirus mutants identify surface and internal capsid residues that control interaction with the cell receptor. *EMBO J* 13:5855–5862.
40. Harber J, Bernhardt G, Lu HH, Sgro JY, Wimmer E (1995) Canyon rim residues, including antigenic determinants, modulate serotype-specific binding of polioviruses to mutants of the poliovirus receptor. *Virology* 214:559–570.
41. Liao S, Racaniello VR (1997) Allele-specific adaptation of poliovirus VP1 B-C loop variants to mutant cell receptors. *J Virol* 71:9770–9777.
42. Racaniello VR (1996) The poliovirus receptor: A hook, or an unzipper? *Structure* 4:769–773.
43. Wien MW, Chow M, Hogle JM (1996) Poliovirus: New insights from an old paradigm. *Structure* 4:763–767.
44. McDermott BM, Jr, Rux AH, Eisenberg RJ, Cohen GH, Racaniello VR (2000) Two distinct binding affinities of poliovirus for its cellular receptor. *J Biol Chem* 275:23089–23096.
45. Tsang SK, McDermott BM, Racaniello VR, Hogle JM (2001) Kinetic analysis of the effect of poliovirus receptor on viral uncoating: The receptor as a catalyst. *J Virol* 75:4984–4989.
46. Brandenburg B, *et al.* (2007) Imaging poliovirus entry in live cells. *PLoS Biol* 5:e183.